in ferromagnetic spin ordering.[13] The sign of π spins at the carbenic carbons of which the spin density is the highest in each phenylmethylene unit becomes the same based on the π-spin correlation. The localized n spins at carbenic carbons will align to the same direction based on the one-center exchange interaction, resulting in ferromagnetic spin ordering. The latter interaction is also expected to stabilize the intramolecular ferromagnetic spin state[14] and resembles s-d interaction in ferromagnetic dilute alloys.[15] The above picture of the spin distribution in the polycarbenes is experimentally shown on some lower homologues, i.e., diphenylmethylene and *m*-phenylenebis(phenylmethylene), by ENDOR measurement.[16]

Although the ferromagnetically spin ordered state is the ground state for the polycarbenes of finite chain length, it is well-known that the ferromagnetic spin ordering in the pure one-dimensional system is destroyed by the thermal excitation of magnon.[17] Therefore, the next step to approach macroscopic ferromagnetism is to introduce ferromagnetic intermolecular interaction among high-spin polycarbenes, regarding them as a microdomain in ferromagnets. Here McConnell's theory on the intermolecular magnetic interaction among the spin distributed π system will serve as the guiding principle.[2a,18] The magnetic susceptibility measurement is expected to be a powerful technique in investigating intermolecular magnetic interaction and macroscopic magnetic properties.

Acknowledgment. The authors are grateful to Dr. K. Nasu of the Institute for Molecular Science for helpful discussions. They are also indebted to S. Murata of the Institute for his skillful help in performing the nonlinear least-squares calculations.

Registry No. 1, 85566-03-6; **2**, 85566-04-7.

(13) Maynau, D.; Said, M.; Malrieu, J. P. *J. Am. Chem. Soc.* **1983**, *105*, 5244.
(14) Magnetic property of the polycarbenes is theoretically predicted by a periodical Kondo-Hubbard model. See: Nasu, K. *Phys. Rev. B*, to be published.
(15) (a) Zener, C. *Phys. Rev.* **1951**, *83*, 299. (b) Ruderman, M. A.; Kittel, C. *Phys. Rev.* **1954**, *96*, 99. (c) Kasuya, T. *Prog. Theor. Phys.* **1956**, *16*, 45. (d) Yoshida, K. *Phys. Rev.* **1957**, *106*, 893.
(16) (a) Hutchison, C. A., Jr.; Kohler, B. E. *J. Chem. Phys.* **1969**, *51*, 3327. (b) Anderson, R. J. M.; Kohler, B. E. *J. Chem. Phys.* **1976**, *65*, 2451. (c) Takui, T.; Kita, S.; Takahashi, T.; Itoh, K. *J. Chem. Phys.*, to be published.
(17) One-dimensional inorganic ferromagnets have been reported. Antiferromagnetic interchain interaction stabilizes the ferromagnetic spin ordering within a chain. See: (a) Mermin, N. D.; Wagner, H. *Phys. Rev. Lett.* **1966**, *17*, 1133. (b) Steiner, M.; Villain, J.; Windsor, C. G. *Adv. Phys.* **1976**, *25*, 87. (c) Rosinski, Ch.; Elschner, S. *J. Magn. Magn. Mater.* **1977**, *4*, 193.
(18) Intramolecular ferro- and antiferromagnetic interactions in bis(phenylmethylenyl)[2.2]paracyclophanes are reported as a model for intermolecular magnetic interaction between two oriented triplet dipehnylcarbenes. See: Izuoka, A.; Murata, S.; Sugawara, T.; Iwamura, H. *J. Am. Chem. Soc.* **1985**, *107*, 1786. Design of intermolecular ferromagnetic interaction has been partly achieved for bis(*p*-octyloxyphenyl)carbene generated in a neat crystal of the corresponding diazo compound. See: Sugawara, T.; Murata, S.; Kimura, K.; Iwamura, H.; Sugawara, Y.; Iwasaki, H. *J. Am. Chem. Soc.* **1985**, *107*, 5293.

Ab Initio Quantum-Chemical Study of the Unimolecular Pyrolysis Mechanisms of Formic Acid†

P. Ruelle,* U. W. Kesselring, and Hô Nam-Tran

Contribution from the School of Pharmacy, University of Lausanne, CH-1005 Lausanne, Switzerland. *Received July 23, 1985*

Abstract: The mechanisms of the two unimolecular competing reactions occurring during the pyrolysis of formic acid have been investigated by ab initio methods by using a variety of basis sets. The effects of valence electron correlation were included by Møller-Plesset (MP) perturbation theory to the fourth order. To explain the apparent inconsistency of the kinetic results, i.e., the lowest activation energy value for the decarboxylation process vs. the dehydration one and a CO/CO_2 ratio of product yield of 10, a new reaction mechanism has been proposed. That is, if the dehydration constitutes the main channel of formic acid pyrolysis with a calculated transition barrier of 67.1 kcal mol^{-1}, then some of the produced water molecules could serve as catalysts for the decarboxylation reaction, the computed activation energy of which amounts to 48.7 kcal mol^{-1}. The observed product ratio can furthermore be explained by the dependence of the decarboxylation process on the dehydration reaction.

I. Introduction

There are relatively few experimental investigations on the thermal decomposition of lower alkanoic acids the pyrolysis of which occurs by two parallel molecular eliminations, i.e., dehydration and decarboxylation. In the case of formic acid[1-4] the only products obseved are CO, H_2O, CO_2, and H_2 from the simultaneous decompositions, the decarboxylation reaction being a relatively minor process with the ratio CO/CO_2 amounting typically to 10.[2]

$$HCOOH \rightarrow CO + H_2O \quad (1)$$

$$HCOOH \rightarrow CO_2 + H_2 \quad (2)$$

By studies of gas-phase kinetics in both batch and flow systems between 457 and 780 °C, Blake et al.[2] found that decarboxylation was a first-order reaction over the whole temperature range ($k_2 = 10^{12.47} \exp(-48.5 \text{ kcal mol}^{-1}/RT)\ s^{-1}$), whereas the rate constant

† Presented at the International Conference on Theory of Organic Reactions (TOR85) held at Gargnano, Italy, in June 1985.

(1) Blake, P. G.; Hinshelwood, C. *Proc. R. Soc. London, A* **1960**, *255A*, 444.
(2) Blake, P. G.; Davies, H. H.; Jackson, G. E. *J. Chem. Soc. B* **1971**, 1923.
(3) Hsu, D. S. Y.; Shaub, W. M.; Blackburn, M.; Lin, M. C. "The Nineteenth International Symposium on Combustion"; the Combustion Institute: Pittsburgh, 1983; p 89.
(4) Saito, K.; Kakumoto, T.; Kuroda, H.; Torii, S.; Imamura, A. *J. Chem. Phys.* **1984**, *80*, 4989.

0002-7863/86/1508-0371$01.50/0

for dehydration exhibited a curved Arrhenius plot. Fitting this experimental curve by the superposition of two straight-line plots, they showed that, at temperatures below 600 °C, the rate constant for dehydration was of second order ($k_1 = 10^{11.44}$ exp(−31.7 kcal mol^{-1}/RT) cm^3 mol^{-1} s^{-1}) tending to 1.5th order ($k_1 = 10^{15.39}$ exp(−60.5 kcal mol^{-1}/RT) s^{-1}) at temperatures above 670 °C. More recently, Hsu et al.[3] studied the thermal decomposition of formic acid highly diluted in Ar by using a shock tube over the temperature range of 1010–1760 °C. By the analysis of the concentration profiles, they determined second-order rate constants for the dehydration and decarboxylation, and they estimated the threshold energies to be 62–65 kcal mol^{-1} for the dehydration and 65–68 kcal mol^{-1} for the decarboxylation.

Although it seems clear that neither dehydration nor decarboxylation involve free-radical chains and that all reactions are homogeneous and molecular, the mechanisms and the rates are still ambiguous as stated by Saito et al.[4] That is, if the threshold energies of the two competing molecular pathways are close to each other within a few kcal mol^{-1}, it is hard to explain the large difference between the CO and CO_2 yields. To elucidate the problem, Saito et al. determined, at the ab initio level, the structures of the molecules along the two reaction pathways. Their lowest activation energies amount respectively to 67.5 and 88.9 kcal mol^{-1} for the dehydration and decarboxylation processes. As for the observed product ratio, such a relative activation energy difference between the two processes (19.5 kcal mol^{-1}) would support the experimental results; i.e., the dehydration consists of the main channel of the thermal formic acid decomposition. However, the 88.9 kcal mol^{-1} decarboxylation activation energy value is neither consistent with Hsu's threshold energy estimation nor does it correspond to any experimental value of that process.

The present study proposes, on the basis of ab initio calculations, a new reaction mechanism which could account for the apparent inconsistency of the experimental results. That is, if we consider that the dehydration reaction constitutes the main channel in the pyrolysis of formic acid, then some of the produced water molecules could serve as catalysts in a water-catalyzed decarboxylation reaction. In this work, only the unimolecular mechanisms of both dehydration and decarboxylation have been investigated.

II. Computational Methods

The energy calculations were carried out by the ab initio method of Roothaan[5] with the MONSTERGAUSS program.[6] Throughout this work, a variety of basis sets ranging in quality from minimal to split-valence, including polarization functions, were used for the optimization of all geometrical parameters. The molecular geometries of the stationary points have been optimized by the force method[7] with use of the analytical gradient. The Optimally Conditioned (OC) technique[8] was employed for searching the minima or minimizing the energies. The transition states were located by minimizing the gradient norm less than 0.0005 mdyn while ensuring that the matrix of second derivatives had only one negative eigenvalue. The Hessian matrices were computed by gradient differences with use of the VA05AD method.[9]

To go beyond the SCF level of theory, the effect of valence electron correlation was incorporated at the level of second (MP2), third (MP3), and fourth (MP4) order Møller–Plesset perturbation theory[10] with different basis sets and optimized geometries. MP4 was treated in the space of single, double, and quadruple substitutions, i.e., MP4(SDQ), relative to a closed-shell HF wave function. These last calculations were performed with GAUSSIAN-80 and GAUSSIAN-82 programs.[11-12]

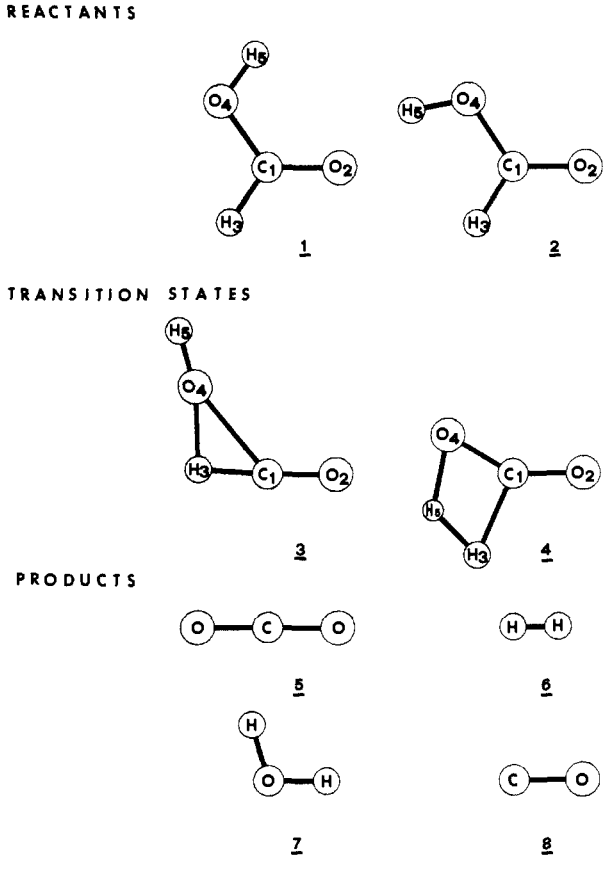

Figure 1. Optimized geometries of the stationary points that are relevant in the study of the formic acid pyrolysis.

III. Results and Discussion

To describe the two reaction mechanisms occurring in the pyrolysis of formic acid, we have identified eight stationary points on the relevant energy surface: two HCOOH conformers (syn and anti), two transition states (a three- and a four-center transition state corresponding respectively to the dehydration and decarboxylation reaction), and four product molecules H_2O, CO, H_2, and CO_2. The structures and the optimized geometrical parameters of the eight stationary points are given in Figure 1 and Table I. All these structures are found to be planar.

The concerted mechanism of dehydration assumes a 1,2-shift of the H_3 atom to the O_4 atom of the OH carboxylic group via a three-center transition state **3** in which the formation of the O–H bond and the breaking of the C–H and C–O bonds take place simultaneously. However, the variation of these bond lengths in the transition state with respect to their equilibrium values in formic acid differs upon basis sets (Table II). The more elongated the C_1–H_3 bond is, the less the increase of the C_1–O_4 bond will be. At the STO-3G level, the C_1–H_3 interatomic distance is more lengthened than the C_1–O_4 bond, and the transition state looks like a charge transfer complex between CO and H_2O molecules with a O═C···OH_2 structure. The magnitude of the charge transferred amounts to 0.101 e$^-$ from the water to the carbon monoxide moiety. On the other hand, at the 6-31G** level of calculation, an opposite situation is observed with a C_1–O_4 bond much more elongated than the C_1–H_3 distance. In this case, the transition state resembles more so a hydrogen-bonded complex with a O═C···HOH structure in which the carbon monoxide and the water molecules are respectively the electron donor and acceptor. The extent of the charge transferred in the transition state from the carbon monoxide to the water moiety is 0.156 e$^-$. Such structure differences upon basis sets can partly be explained by the representation of the dipole moment of CO. It is a well-known

(5) Roothaan, C. C. J. *Rev. Mod. Phys.* **1951**, *23*, 69.

(6) Peterson, M. R.; Poirier, R. A.; Csizmadia, I. G. "Program MONSTERGAUSS", Department of Chemistry, University of Toronto, Toronto, 1980.

(7) Schlegel, H. B. *J. Comput. Chem.* **1982**, *3*, 214.

(8) Davidon, W. C. *Math. Prog.* **1975**, *9*, 1.

(9) Powell, M. J. D. "Program VA05AD", Harwell Subroutine Library, Atomic Energy Research Establishment, Harwell, UK.

(10) Møller, C.; Plesset, M. S. *Phys. Rev.* **1934**, *46*, 618.

(11) Binkley, J. S.; Whiteside, R. A.; Krishnan, R.; Seeger, R.; Defrees, D. J.; Schlegel, H. B.; Topiol, S.; Kahn, L. R.; Pople, J. A. "Program GAUSSIAN-80"; *QCPE* 1981; Vol. 13, p 406.

(12) Binkley, J. S.; Frisch, M. J.; Defrees, D. J.; Raghavachari, K.; Whiteside, R. A.; Schlegel, H. B.; Fluder, E. M.; Pople, J. A. "Program GAUSSIAN-82"; Carnegie Mellon University, Philadelphia, PA, 1983.

Table I. Ab Initio Optimized Structures of the Stationary Points for the Formic Acid Uncatalyzed Decomposition[a]

molecule	parameter	STO-3G	3-21G	4-31G	6-31G	6-311G	6-31G*	6-31G**
formic acid	C1–O2	1.214	1.198	1.200	1.204	1.202	1.182	1.182
syn **1**	C1–O4	1.385	1.350	1.342	1.345	1.341	1.323	1.321
	C1–H3	1.103	1.074	1.072	1.073	1.072	1.083	1.085
	O4–H5	0.990	0.969	0.956	0.955	0.951	0.953	0.949
	H3–C1–O2	126.0	125.8	124.9	124.9	124.9	124.7	124.7
	O4–C1–O2	123.6	124.6	124.6	124.4	124.3	124.9	124.8
	H5–O4–C1	104.7	112.7	114.9	114.9	114.6	108.7	108.9
formic acid	C1–O2	1.211	1.192	1.193	1.197			1.176
anti **2**	C1–O4	1.392	1.354	1.346	1.350			1.327
	C1–H3	1.107	1.082	1.080	1.081			1.091
	O4–H5	0.988	0.962	0.951	0.950			0.944
	H3–C1–O2	124.2	123.6	122.9	122.9			123.1
	O4–C1–O2	121.3	122.6	122.5	122.3			123.0
	H5–O4–C1	105.8	114.8	116.6	116.7			111.7
three-center	C1–O2	1.186	1.141	1.133	1.135	1.129	1.114	1.117
transition state	C1–O4	1.533	1.748	1.840	1.848	1.863	1.881	1.846
3	C1–H3	1.310	1.212	1.172	1.169	1.163	1.166	1.165
	O4–H3	1.176	1.286	1.348	1.357	1.369	1.369	1.351
	O4–H5	0.999	0.973	0.955	0.954	0.949	0.952	0.946
	O2–C1–O4	121.6	126.8	128.5	128.5	128.7	130.2	129.4
	O4–C1–H3	48.1	47.7	47.0	47.1	47.1	46.4	46.9
	H3–O4–H5	161.1	162.2	163.3	163.3	163.3	162.4	164.6
four-center	C1–O2	1.174	1.144	1.150	1.154			1.147
transition state	C1–O4	1.305	1.266	1.266	1.271			1.235
4	C1–H3	1.586	1.657	1.570	1.559			1.454
	O4–H5	1.204	1.227	1.269	1.276			1.259
	H3–H5	0.988	1.123	1.085	1.076			1.023
	O4–C1–O2	155.5	152.8	150.7	150.7			149.1
	H3–C1–O4	85.3	88.4	91.4	91.7			97.2
	C1–O4–H5	76.8	81.2	77.6	76.9			70.1
	C1–H3–H5	70.3	68.4	70.8	71.3			68.1
	H3–H5–O4	127.6	121.9	120.1	120.1			124.5
CO_2 **5**	C–O	1.188	1.156	1.158	1.161			1.143
H_2 **6**	H–H	0.712	0.735	0.730	0.730			0.732
H_2O **7**	O–H	0.989	0.967	0.951	0.949	0.945	0.947	0.943
	H–O–H	100.0	107.7	111.2	111.6	111.9	105.5	106.0
CO **8**	C–O	1.145	1.129	1.128	1.131	1.124	1.114	1.114

[a] Bond length in angstroms; bond angle in degrees.

Table II. Variation of the Bond Lengths (Angstroms) in the Three-Center Transition State with Respect to Their Equilibrium Value in the Syn Formic Acid Molecule

parameter	STO-3G	3-21G	4-31G	6-31G	6-311G	6-31G*	6-31G**
ΔC1–H3	0.207	0.138	0.100	0.096	0.091	0.083	0.080
ΔC1–O4	0.148	0.398	0.498	0.503	0.522	0.558	0.525

fact that at the Hartree–Fock level, the sign of the dipole moment of CO is incorrectly given as $^{+}C{=}O^{-}$.[13] A quite similar problem has also been encountered in the ab initio molecular orbital studies of the most stable intermolecular complex structure between CO and HF.[14,15] In their works dealing with the structures and energetics of the isomeric H-bonded complexes OC···HF and CO···HF, Curtiss et al[15] have shown that the relative stability of these structures is very dependent upon basis sets and inclusion of correlation effects. Whereas the 6-31G* basis set already predicts the right structure, only the inclusion of electron correlation gives a significant preference for the experimentally observed OC···HF isomer.[16-17] In this case, the authors argued that the large effect of correlation upon the relative stability of the two isomers was apparently entirely an electrostatic effect caused by the correlation-induced sign reversal of the dipole moment of CO. This suggests that the values of the geometrical parameters of transition state **3** could still be improved by performing a geometry

Table III. Relative Energies for the Formic Acid Dehydration Reaction[a]

method	E^{act}	ΔE^{react}
HF/STO-3G//HF/STO-3G	117.98	16.65
HF/3-21G//HF/3-21G[4]	85.0	13.14
HF/4-31G//HF/4-31G[4]	82.6	9.17
HF/6-31G//HF/6-31G[4]	82.3	8.10
HF/6-311G//HF/6-311G	82.27	5.87
HF/6-31G*//HF/6-31G*	96.43	8.59
HF/6-31G**//HF/6-31G**	93.32	5.69
MP2/6-31G//HF/6-31G[4]	67.5	7.96
MP2/6-31G//HF/6-311G	67.77	8.51
MP3/6-31G//HF/6-311G	76.29	11.32
MP4/6-31G//HF/6-311G	70.93	8.46
MP2/6-31G**//HF/6-31G**	80.69	12.63
MP2/6-311G//HF/6-311G	67.06	5.60
exptl	60.05[2] 62–65[3]	8.31[4]

[a] kcal mol^{-1}.

(13) Grimaldi, F.; Lecourt, A.; Moser, C. *Int. J. Quantum Chem., Symp.* **1967**, *2*, 106.
(14) Benzel, M. A.; Dykstra, C. E. *Chem. Phys.* **1983**, *80*, 273.
(15) Curtiss, L. A.; Pochatko, D. J.; Reed, A. E.; Weinhold, F. *J. Chem. Phys.* **1985**, *82*, 2679.
(16) Legon, A. C.; Soper, P. D.; Flygare, W. H. *J. Chem. Phys.* **1981**, *74*, 4944.
(17) Andrews, L.; Arlinghaus, R. T.; Johnson, G. L. *J. Chem. Phys.* **1983**, *78*, 6347.

Table IV. Relative Energies for the Formic Acid Decarboxylation Reaction[a]

method	ΔE^{rot}	E^{act}	$E^{act}_{H_2O}$	ΔE^{react}
HF/STO-3G//HF/STO-3G	4.43	131.80	76.66	20.07
HF/3-21G//HF/3-21G	7.20	106.40[4]	54.99	10.03
HF/4-31G//HF/4-31G	6.90	112.70[4]	65.97	13.05
HF/6-31G//HF/6-31G	6.80	114.40[4]	68.01	14.89
HF/6-31G**//HF/6-31G**	6.00	95.98	67.83	3.17
MP2/6-31G//HF/6-31G	6.30	88.90	47.83	-4.44
MP2/6-31G**//HF/6-31G**	5.60	77.61	48.70	-1.65
exptl	4.0[19]		48.5[2] 65-68[3]	-1.36[4]

[a] kcal mol^{-1}.

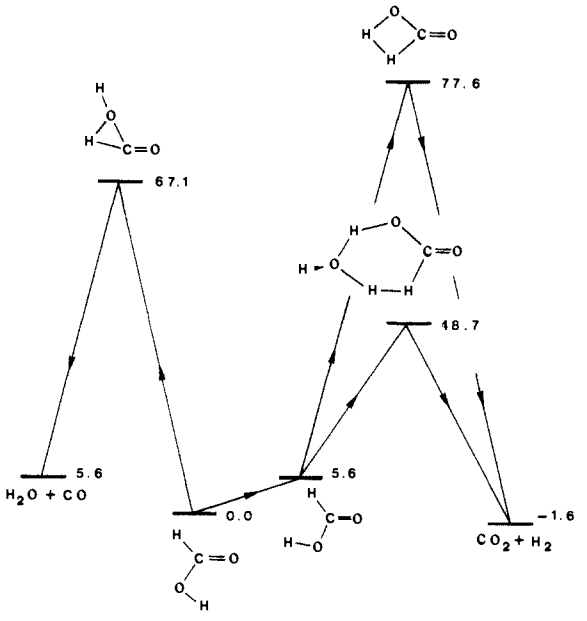

Figure 2. Energy diagrams for the unimolecular pyrolysis mechanisms of formic acid. MP2/6-311G//HF/6-311G values for the dehydration pathway and MP2/6-31G**//HF/6-31G** values for the decarboxylation pathway. (Energies are given in kcal mol^{-1}.)

optimization at the MP level of calculation.

The mechanism of formic acid decarboxylation yielding H_2 and CO_2 assumes at first a conformational change from the most stable syn structure of formic acid **1** to the less stable anti conformer **2**. Peterson and Csizmadia[18] have made a complete analysis of the conformational hypersurface of formic acid, and they calculated a barrier to rotation of 9.61 kcal mol^{-1}. From that intermediate, the decarboxylation proceeds via a four-membered transition state **4** by simultaneous C_1–H_3 and O_4–H_5 bond cleavages and H_3–H_5 bond formation. Contrary to the previous dehydration process, the overall transition-state structure is quite similar in all the basis sets used.

Tables III and IV summarize the Hartree–Fock and perturbative relative energies for the stationary points of respectively dehydration and decarboxylation pathways at all levels of calculation. All the energies given in those tables are relative to those of the reactant, i.e., the syn formic acid conformer **1**. The energy profiles corresponding to those two competing reactions are shown in Figure 2. The values indicated in this figure correspond to the MP2/6-311G//HF/6-311G and MP2/6-31G**//HF/6-31G** results respectively for the dehydration and decarboxylation pathways. First of all, it can be seen that at the SCF level, the STO-3G activation energy values of the two processes are greatly overestimated.

With respect to the decarboxylation reaction, as it can be expected, both addition of polarization functions and correlation effects lower the activation energy. However, for the dehydration process, addition of d polarization functions increases the activation energy value which is descreased by p polarization functions and correlation effects. Such a behavior had already been reported by Oie et al.[20-23] in an extensive theoretical study on the reaction between ammonia and formic acid.

Compared to the experimental results, we find that for the dehydration process, only the activation energies (67 kcal mol^{-1}) calculated at the MP2 level with nonpolarized basis sets agree with the value obtained by Blake et al. (60.5 kcal mol^{-1}) and with the threshold energy estimated by Hsu (62–65 kcal mol^{-1}). Nevertheless, with regard to the previously mentioned structural considerations on the three-center transition state, a still better agreement could probably be obtained by performing the geometry optimization at the MP level.

As for the relative energies of the transition state associated with the decarboxylation mechanism, all of them, even at the most sophisticated level of calculation, are too high and do not correspond to any experimental value. At this stage, it should be remembered that dehydration constitutes the main channel in the pyrolysis of formic acid. Thus, we have reexamined the reaction pathway of decarboxylation but this time catalyzed by a water molecule originating from the most important reaction of the pyrolysis. Figure 3 and Table V reproduce respectively the structure and the optimized geometrical parameters of the water-catalyzed transition-state **9**. In that transition state the structure of which is a nearly six-membered ring, the role of the water molecule is to serve as a proton relay acting simultaneously as a hydrogen atom donor and acceptor while preserving its

Table V. Ab Initio Optimized Structure of the Six-Membered Ring Transition State for the Formic Acid Water-Catalyzed Decarboxylation[a]

parameter	STO-3G	3-21G	4-31G	6-31G	6-31G**
C1-O2	1.195	1.175	1.186	1.192	1.169
C1-O4	1.255	1.225	1.224	1.227	1.207
C1-H3	1.534	1.497	1.417	1.409	1.411
O4-H5	1.337	1.548	1.797	1.865	1.719
H5-O6	1.054	1.019	0.974	0.967	0.976
O6-H8	0.983	0.965	0.949	0.947	0.949
O6-H7	1.195	1.166	1.155	1.157	1.142
H3-H7	0.935	1.071	1.061	1.052	1.071
O4-C1-O2	146.8	145.8	144.5	144.4	144.7
O4-C1-H3	104.8	106.0	108.0	108.2	109.0
C1-O4-H5	108.0	113.4	114.1	114.1	110.8
O4-H5-O6	153.4	138.8	122.8	118.8	133.1
H5-O6-H7	86.1	94.4	103.4	106.0	93.3
O6-H7-H3	154.6	152.8	156.8	158.0	160.9
C1-H3-H7	113.0	114.0	114.7	114.8	112.5
H5-O6-H8	105.5	116.6	121.9	122.5	110.1
H8-O6-H5-O4	103.9	118.6	152.5	166.7	110.7

[a] Bond length in angstroms; bond angle in degrees.

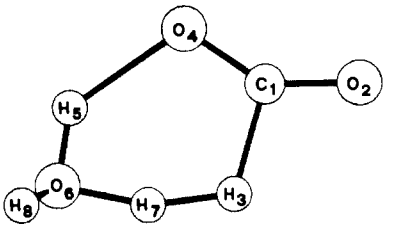

9

Figure 3. Optimized geometry of the six-membered ring transition state for the water-catalyzed decarboxylation process of formic acid.

(18) Peterson, M. R.; Csizmadia, I. G. *J. Am. Chem. Soc.* **1979**, *101*, 1076.

(19) Lide, D. R. *Trans. Am. Crystallogr. Assoc.* **1966**, *2*, 106.

(20) Oie, T.; Loew, G. H.; Burt, S. K.; Binkley, J. S.; MacElroy, R. D. *J. Am. Chem. Soc.* **1982**, *104*, 6169.

(21) Oie, T.; Loew, G. H.; Burt, S. K.; Binkley, J. S.; MacElroy, R. D. *Int. J. Quantum Chem., Quantum Biol. Symp.* **1982**, *9*, 223.

(22) Oie, T.; Loew, G. H.; Burt, S. K.; MacElroy, R. D. *J. Am. Chem. Soc.* **1983**, *105*, 2221.

(23) Oie, T.; Loew, G. H.; Burt, S. K.; MacElroy, R. D. *J. Comput. Chem.* **1983**, *4*, 449.

identity. The transfer of the H_7 hydrogen atom from the water molecule to the H_3 hydrogen atom to form the hydrogen product molecule occurs in a concerted way with the transfer of the H_5 hydrogen atom from the hydroxyl group to the O_6 oxygen atom regenerating thus a new water molecule. The activation energy of this process obtained at the different levels of calculation are given in the fourth column of Table IV. The comparison of the third and fourth column of that table shows clearly the catalytic effect of the water molecule amounting to about 50 kcal mol^{-1} at the STO-3G and 3-21G levels and to 28 kcal mol^{-1} at the 6-31G** level. Compared with the effect of the polarization functions which do not lower the activation energy, the contribution of electron correlation effects is fairly large and must, therefore, be taken into account for a correct description of the reaction pathway. In fact, at the MP2 6-31G** level, both the calculated activation and reaction energies coincide with the experimental values, respectively 48.5 and −1.36 kcal mol^{-1}. Moreover, one can observe that only the activation energy related to the water-catalyzed decarboxylation mechanism corresponds to the experimental one. That decarboxylation should be catalyzed by a water molecule does not seem inconsistent with the experimental facts since the main channel of the formic acid pyrolysis yields water. Furthermore, given the two mechanisms, the ratio observed in the product yield, i.e., CO/CO_2, could simply be due to the dependence of the decarboxylation on the dehydration reaction and also on the number of effective collisions between the remaining formic acid and the produced water molecules in the gaseous state. From the experimental point of view, this result would suggest that the product ratio could be modified by introducing simultaneously the formic acid and some water vapor into the reactor.

Finally, the large difference between Hsu's decarboxylation activation energy and the one found here and by Blake probably lies in Hsu's kinetic treatment. He determined a second-order rate constant for the decarboxylation in opposition with the first-order rate found by Blake.

Acknowledgment. This work is part of a project funded by the Swiss National Foundation for Scientific Research (Grant No. 3.654-0.84). We gratefully acknowledge the generous assistance of the Centre de Calcul de l'Ecole Polytechnique Fédérale de Lausanne. We express our thanks to Professor J. Weber from the University of Geneva and to Dr. G. Dive from the University of Liège who carried out the MP calculations.

Registry No. Formic acid, 64-18-6.

Photochemistry and Radiation Chemistry of Colloidal Semiconductors. 12. Intermediates of the Oxidation of Extremely Small Particles of CdS, ZnS, and Cd_3P_2 and Size Quantization Effects (A Pulse Radiolysis Study)

S. Baral, A. Fojtik,† H. Weller, and A. Henglein*

Contribution from the Hahn-Meitner-Institut für Kernforschung Berlin, Bereich Strahlenchemie, D-1000 Berlin 39, Federal Republic of Germany. *Received August 7, 1985*

Abstract: The reactions of hydroxyl radicals with colloidal Q-CdS, Q-ZnS, and Q-Cd_3P_2 (materials of extremely small particle size showing optical size quantization effects) were studied pulse radiolytically. The radicals attack the particles at diffusion-controlled rates. In all three cases, a product with a broad absorption band in the visible (sulfides) or near-infrared (phosphide) is formed. This band shifts to shorter wavelengths with decreasing particle size (size quantization effect). It is attributed to surface trapped holes. These holes react with dissolved oxygen. The colloidal particles become a little smaller by OH attack. With use of a CdS sample with a structured absorption spectrum, it is shown that the product particles have their absorption maxima at slightly shorter wavelengths than the reactant particles (size quantization effect).

Radiation chemical studies on colloidal solutions of semiconductor materials allow one to investigate interfacial reactions of free radicals. The radicals are formed in bulk solution and transfer an electron to the colloidal particles. This electron transfer may lead to a cathodic dissolution of the colloid, such as in the case of silver halides.[1] The transferred electrons may be stored for some time and produce a colored material, such as blue TiO_2,[2] or reduce another solute in a two-electron-transfer process.[3] Studies of this kind complement the studies on the photochemistry of such solutions. In the latter case, electrons and positive holes are generated by light absorption and the chemical reactions, which are initiated by these charge carriers, are investigated. The advantage of using radicals for the transfer of electrons is that excess electrons on small particles can be studied without positive holes being present simultaneously.[4,5]

In the present studies, OH radicals are used to inject positive holes into semiconductor particles possessing anions such as S^{2-} and P^{3-} which are readily oxidized. The anodic corrosion is a disturbing problem in the electrochemistry and photoelectrochemistry of compact semiconductor electrodes.[6] To generate OH radicals, colloidal solutions containing nitrous oxide were irradiated. Using the method of pulse radiolysis, one obtains information on the rate of OH attack and on the optical properties and lifetimes of the first intermediates of corrosion. The optical detection of intermediates at compact electrodes is not possible in most cases as the number of species produced in electrochemical experiments is too low. The experiments with colloidal particles

†Home address: Czechoslovak Academy of Sciences, J. Heyrovský Institute of Physical Chemistry and Electrochemistry, Prague, CSSR.

(1) Johnston, F. J. *Rad. Res.* **1978**, *75*, 286-295.
(2) Henglein, A. *Ber. Bunsenges. Phys. Chem.* **1982**, *86*, 241-246.
(3) Gutiérrez, M.; Henglein, A. *Ber. Bunsenges. Phys. Chem.* **1983**, *87*, 474-478.
(4) Henglein, A. In "Photochemical conversion and storage of solar energy"; Rabani, J., Ed.; The Weizmann Science Press of Israel, 1982; Part a, pp. 115-138.
(5) Henglein, A. In "Modern trends of colloid science in chemistry and biology"; Eicke, F., Ed.; Birkhäuser Verlag: Basel, 1985; pp 126-147.
(6) Gerischer, H. "Advances in Electrochemistry and Electrochemical Engineering"; Delahay, P., Ed.; Interscience Publishers: New York, 1961; pp 1, 139-232.

0002-7863/86/1508-0375$01.50/0